Applied Thermal Engineering 173 (2020) 115183

Contents lists available at ScienceDirect

Applied Thermal Engineering

journal homepage: www.elsevier.com/locate/apthermeng

Experimental study of heat transfer capacity for loop heat pipe with flat disk evaporator

Zikang Zhang, Hao Zhang, Zhenyuan Ma, Zhichun Liu, Wei Liu*

School of Energy and Power Engineering, Huazhong University of Science and Technology, Wuhan 430074, China

HIGHLIGHTS

- An ammonia LHP with flat evaporator and long heat transfer distance was designed.
- The loop could operate stably in the range of heat loads from 2.5 W to 180 W.
- The evaporator inlet temperature suffered a staged decline due to vapor expansion.
- Two different processes related to vapor phase and heat leak were observed.
- A minimum LHP thermal resistance was 0.252 °C/W at heat sink temperature of 10 °C.

ARTICLE INFO

Keywords:
Loop heat pipe
Flat disk evaporator
Biporous wick
Long heat transfer distance
Performance experiment

ABSTRACT

Loop heat pipes are passive heat transfer devices which can meet the heat dissipation requirement of high-power electronic devices in aerospace and terrestrial applications. This paper investigates the operating characteristic of a stainless steel-ammonia loop heat pipe with a flat disk evaporator. A biporous wick made from sintered nickel powders was used to produce the capillary force. The heat transfer distance was 1.6 m and the allowable heater surface temperature was below 70 °C. Tests demonstrated that the loop could operate under a heat load ranging from 2.5 W to 180 W (heat flux 0.15–10.8 W/cm^2) at heat sink temperature of −10 °C. In addition, variable conductance mode and constant conductance mode existed, and no obvious temperature overshoot or pulsation was observed. The evaporator inlet temperature went through a staged decline due to the effect of initial driving force of vapor expansion during the start-up process. Meanwhile, under the synergy of heat leaks from heater surface and long transport line, whether the vapor phase would form inside the compensation chamber could result in a large discrepancy in temperature trends. The minimum evaporator thermal resistance was 0.096 °C/W at heat sink temperature of −10 °C and the minimum LHP thermal resistance was 0.252 °C/W at heat sink temperature of 10 °C.

1. Introduction

Loop heat pipe (LHP) is a passive heat transfer device whose application scenarios cover spacecrafts and terrestrial electronic devices due to its high efficiency and stability [1–5]. By using the capillary mechanism [6], the working fluid can transport heat flux from evaporator to condenser while keeping the circulation inside the loop. Compared with other passive heat transfer devices like traditional heat pipe and capillary pumped loop, LHP has the merits of long heat transfer distances, high heat transfer capability, low thermal resistance and flexible construction implementations.

Since it has many advantages in heat dissipation, a large number of experimental and numerical researches have been carried out to study the working performance and physical mechanism of LHP under various operating conditions. The main components include an evaporator, a condenser, vapor and liquid lines that together form a closed two-phase fluid flow cycle. The capillary structure acted as capillary pump separates the evaporator into two parts, which are named as compensation chamber and evaporation chamber respectively. The subcooled fluid first enters compensation chamber, then pumps towards evaporation chamber and absorbs heat while turning into vapor. Before flowing back to the evaporator, the vapor dissipates heat in condenser and turns into subcooled fluid again. After long-term experimental investigations, the evaporators are either in cylindrical shapes or in flat shapes. However, nearly all of the electronic chips have flat thermo-contact surfaces. Thus, for the cylindrical evaporator LHP, a saddle

* Corresponding author.
E-mail address: w_liu@hust.edu.cn (W. Liu).

https://doi.org/10.1016/j.applthermaleng.2020.115183
Received 18 November 2019; Received in revised form 6 March 2020; Accepted 7 March 2020
Available online 09 March 2020
1359-4311/

Nomenclature

d	pore diameter [m]
k	porous permeability [m^2]
Q	heat load [W]
R	thermal resistance [°C/W]
T	temperature [°C]

Greek symbol

ε	porosity

Subscripts

c	condenser
evap	evaporator
hs	heater surface
v	vapor at evaporator outlet
sink	heat sink

Abbreviations

Amb	ambient
CCM	constant conductance mode
Comp-wall	compensation chamber
Cond-in	condenser inlet
Cond-out	condenser outlet
Evap-in	evaporator inlet
Evap-out	evaporator outlet
HS	heater surface
SS	stainless steel
TC	thermocouple
VCM	variable conductance mode

made of copper or aluminum is needed to ensure a tight contact between evaporator and thermo-contact surface [7,8]. Such an extra component increases the thermal resistance and the mass of the system, reducing the heat transfer capacity eventually. Another disadvantage of the cylindrical evaporator is the nonuniform temperature distribution on thermo-contact surface caused by the uneven thermal path between evaporation interface and heater surface. The flat evaporator LHP can solve the above problems. It has a flat thermo-contact surface and can be well attached to the electronic devices [9]. Besides, the temperature uniformity is improved and the thermal resistance is reduced [10,11].

The majority of efforts have been devoted to the development and improvement of the flat evaporator LHP during recent decades. Singh et al. [12] developed a miniature copper-water LHP with a flat disk shaped evaporator. The lengths of the vapor and liquid lines were 150 mm and 290 mm. The start-up tests indicated that the loop was able to transfer heat load ranging from 5 W to 70 W without working failure. Anand et al. [13] studied the thermal behavior of a miniature flat disk LHP with four working fluids and showed that n-pentane had the lowest operating temperature. Maydanik et al. [14] carried out an analytical review of experiments and simulations of LHP with flat evaporator. Conclusions were made by numerous results that the most efficient combination for temperature below 70 °C was stainless steel-nickel-ammonia and for temperature above 70 °C was copper-copper-water. Odagiri et al. [15] tested a flat rectangular evaporator LHP on high heat flux with different orientations. Result was found that once the wick contacted the vapor phase in liquid core, the heat leakage to the compensation chamber and pressure drop in the wick would become large. Kiseev et al. [16] investigated the optimization of the physical and geometrical parameters of the flat capillary wick. A correct choice of the vapor grooves configuration and fine porous wick thickness would be necessary for the evaporator optimization. A copper-water LHP with a flat square evaporator designed by Li et al. [17] was studied at vertical orientation. The maximum heat load was 450 W and the heat transfer distance (vapor line length) was 120 mm. Two operation modes, boiling trigger start-up and evaporation trigger start-up, were proposed to illustrate the operating characteristics when the LHP was subjected to different heat loads. He et al. [18] designed a stainless steel-ammonia LHP with a secondary wick inserted in compensation chamber. With the combination of the primary wick and the secondary wick, the effect of non-condensable gas was minimized and the temperature oscillation was restrained. Boo et al. [19] developed a small-scale LHP with polypropylene wick. The evaporator was made of stainless steel and the vapor/liquid lines were both 500 mm. Best results were concluded with methanol at a horizontal orientation, and the maximum heat load was 80 W at evaporator temperature of 90 °C.

By using the biporous wick, the LHP heat transfer capacity can get a certain level of promotion. Semenic et al. [20,21] measured the thermophysical properties of different biporous wicks and monoporous wicks. Results illustrated an enhancement in critical heat flux owing to bigger evaporating menisci in biporous wick. Cao et al. [22] compared three bidispersed wick structures to two monodispersed wick structures and found that the heat transfer coefficient and the critical heat flux are all increased. Also there existed an optimal large/small pore diameter ratios which gave the best heat transfer performance. Chen et al. [23,24] carried out an experimental investigation of LHP with flat evaporator using biporous wick. The lengths of the vapor and liquid lines were 335 mm and 415 mm. The maximum heat load could reach 130 W at evaporator temperature below 60 °C and the loop showed strong stability without obvious temperature oscillation.

For better reference and comparison, Tables 1 and 2 generalize the main geometric parameters and thermal characteristics of some flat evaporator LHPs mentioned above. The evaporator sizes in Table 1 are the diameter/height for flat disk evaporators and the length/width/height for rectangular evaporators. It can conclude that most of the heat

Table 1
The main geometric parameters of LHPs.

Evaporator	Evaporator sizes, mm	Evaporator/wick material	Working fluid	Vapor + liquid line length/dia., mm	Ref.
Disk 1	40/19	Copper/SS	Methanol	320 + 450/4	[31]
Disk 2	40/18	SS/nickel	Ammonia	330 + 390/(2.5 + 1.5)	[10]
Disk 3	30/12	SS/nickel	Ammonia	320 + 515/2	[18]
Disk 4	43/15	SS/nickel	Ammonia	335 + 415/2	[23]
Disk 5	102/62.5	Aluminum + SS/nickel	Ammonia	1760 + 2310/4.57	[27]
Disk 6	50/13	SS/SS	Water	450 + 900/2	[11]
Disk 7	30/10	Copper/nickel	Water	150 + 290/2	[12]
Rectangle 1	30/30/15	Copper/copper	Water	120 + 120/5	[17]
Rectangle 2	51/68/15	SS/SS	Acetone	110 + 270/4.35	[15]
Rectangle 3	50/40/30	Aluminum/ploypropylene	Methanol	500 + 500/(4 + 2)	[19]

Table 2
The main thermal characteristics of LHPs.

Evaporator	LHP min. thermal resistance, °C/W	Max. heat load, W	Max. heat flux, W/cm^2	LHP position, grad	Ref.
Disk 1	0.26	240	19.1	0	[31]
Disk 2	0.084	300	23.9	−90	[10]
Disk 3	0.337	110	10.8	0	[18]
Disk 4	0.33	130	12.8	0	[23]
Disk 5	0.22	300	4.5	0	[27]
Disk 6	3.33	70	3.9	0	[11]
Disk 7	0.17	80	12.8	0	[12]
Rectangle 1	0.033	450	72.0	−90	[17]
Rectangle 2	0.064	280	19.6	0	[15]
Rectangle 3	0.80	80	6.5	0	[19]

transfer distances, reflected by the vapor line lengths, are around 0.5 m. However, such a short heat transfer distance is not enough for aerospace applications since the electronic devices are always deep inside the satellites. As for the cylindrical evaporator LHP, the wick can generate more evaporating menisci and larger capillary pressure due to its larger cylindrical surface than flat wick. Thus, the heat transfer distance can reach 10 m [25], or even up to 21 m [26]. Though there are certain experiments focusing on increasing the heat transfer distance in flat evaporator [27,28], the maximum heat flux and the heat transfer capacity decreased adversely. Besides, the flat evaporator LHP shows more obvious temperature pulsation compared to those with cylindrical evaporator because of more significant heat leak flowing to the compensation chamber [29,30]. Such temperature pulsation further limits the broad use of the flat evaporator LHP. This paper presents a modified LHP with a flat disk evaporator and a biporous wick. The heat transfer distance was 1.6 m and the allowable heater surface temperature was below 70 °C. A series of investigations including start-up and continuous heat load cycle tests were conducted to obtain the operating performance of the loop. No obvious temperature pulsation was found and three particular phenomena were observed and discussed in detail. The aim of this work was to develop a flat disk LHP that could satisfy both the heat transfer distance and heat transfer capability needed for aerospace electronic devices.

2. Design of experimental setup

2.1. LHP design

The LHP was composed of a flat disk shape evaporator, a condenser, vapor and liquid transport lines. A biporous wick, which was sintered by nickel powder, was used to provide the capillary pressure. Fig. 1(a) and (b) present the wick appearance and scanning electron microscopy photograph. The porosity of the wick was 74.4% and the equivalent pore diameter was about 5.8 μm. The small pores were formed by the nickel particles, and the large pores were formed by dissolving the pore formers. By using Carman-Kozeny formula [32]

$$k = \frac{d^2\varepsilon^3}{180(1-\varepsilon)^2} \quad (1)$$

the wick permeability was about 1.17×10^{-12} m^2. In the above formula, k is the permeability of wick, d is the mean pore diameter, and ε is the wick porosity. Details of the wick fabrication process could be seen in previous work in Ref. [33]. Compared with conventional monoporous wick, large pores in biporous wick could increase the evaporation intensity by enlarging the vapor-liquid interface and decrease the flow resistance through wick, small pores could provide enough capillary force for the system circulation. This combination could substantially reduce the flow resistance while lowering the capillary force loss. The configuration of the evaporator made of SS304 is shown in Fig. 2(a). The outer diameter and total thickness of the evaporator were 60 mm and 25 mm, respectively. The wick diameter was 46.86 mm and the thickness was 2.83 mm. The vapor removal channels (width 1 mm and depth 1 mm) were made on the internal wall of the heating zone. The evaporator wall thickness was 2 mm and six ribs (width 4 mm and depth 3 mm) were fabricated outside of the compensation chamber. Also the evaporator was sealed by laser weld for better pressure-bearing capacity. The double-pipe heat exchanger used as the condenser was 1260 mm in length. The vapor line and liquid line made of SS304 were 1620 mm and 1480 mm in length, respectively. The inner diameters of two transport lines were both 4 mm for small flow resistance. Anhydrous ammonia with a purity of 99.995%

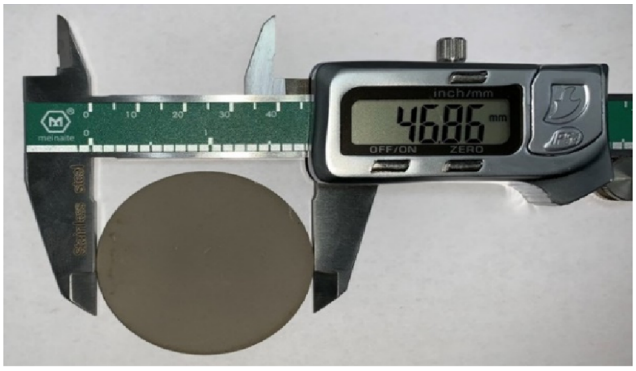

(a)

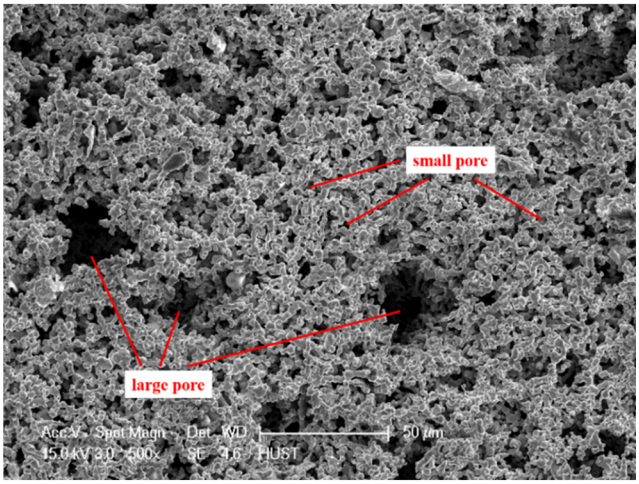

(b)

Fig. 1. (a) The appearance of the wick. (b) Structure of the biporous wick at ×500 magnification.

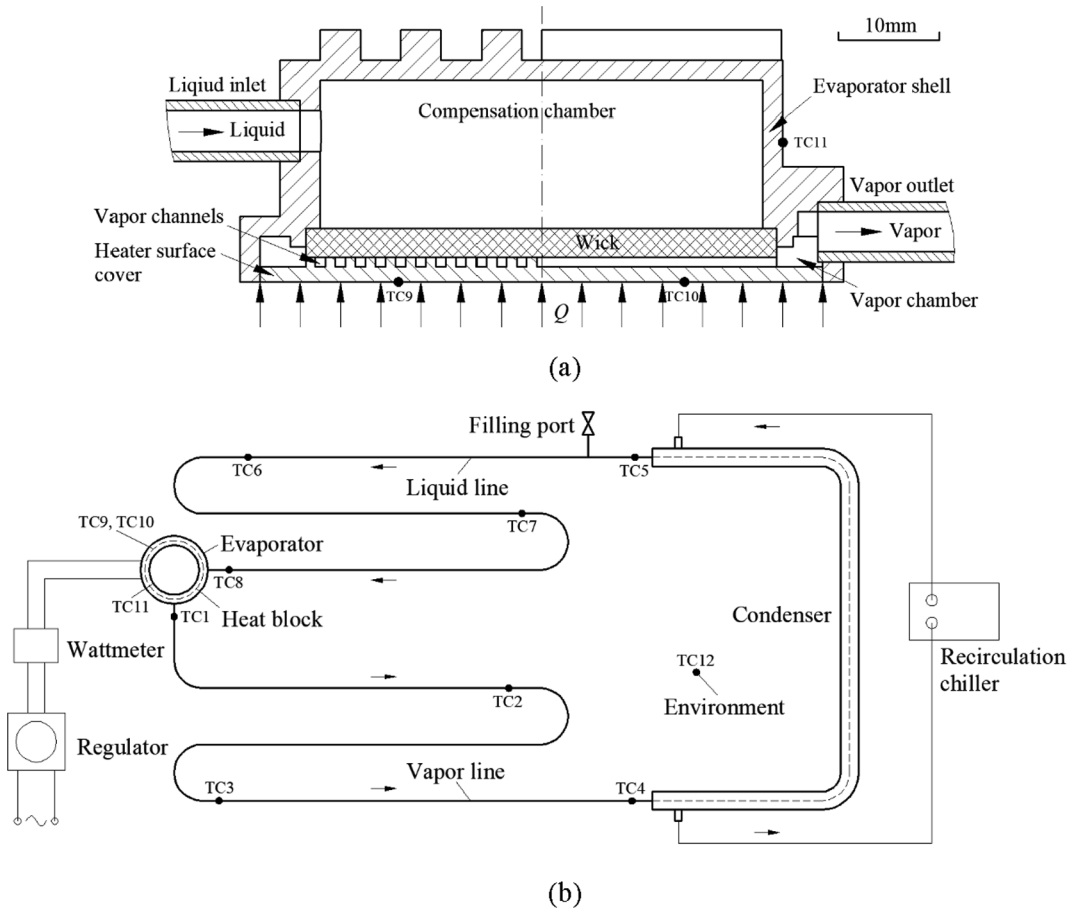

Fig. 2. (a) The configuration of the evaporator. (b) The test schematic of the experimental prototype.

Table 3
The main parameters of the loop components.

Evaporator	Heated diameter	60 mm	Vapor line	Diameter I/O	4/6 mm
	Overall height	25 mm		Length	1620 mm
	Material	SS304		Material	SS304
Compensation chamber	Diameter	48 mm	Liquid line	Diameter I/O	4/6 mm
	Height	14.67 mm		Length	1480 mm
Porous wick	Diameter	46.86 mm		Material	SS304
	Thickness	2.83 mm	Condenser	Inner tube diameter I/O	4/6 mm
	Porosity	74.4%		Outer tube diameter I/O	16/12 mm
	Material	Nickel		Length	1260 mm

was chosen as the working fluid due to its good thermophysical characteristics. However, the operating pressure of the anhydrous ammonia was much higher than other working fluids. Thus, the strength of the evaporator needed to be considered beforehand for experimental safety. Table 3 gives the main parameters of the components and Fig. 3 presents the system diagram of the loop.

2.2. Test methods

In the experiment, a copper heat block with four cartridge heaters embedded was used as the heat source. The heat source diameter was 46 mm and the active heater area was 16.62 cm^2. Heat load was measured by a wattmeter with an accuracy of 0.5%. A special hold-down device and thermal greases were applied to attain a tight contact between the evaporator and heat source. The LHP temperatures were measured by T-type thermocouples with an accuracy of ± 0.5 °C. A data acquisition system "Keithley 2700" connected with a personal computer was used for recording the temperature signals every 3 s. The condenser was cooled by a recirculation chiller with an accuracy of ± 1 °C and the refrigerant used in recirculation chiller was the glycol solution with 50% volume fraction. The evaporator and condenser were on the same level to eliminate the gravity effect. Both the loop and heat block were insulated by using thermal insulation material (PVC/NBR, Fuerda, thermal conductivity 0.034 W/m·K) to reduce the heat loss to ambient. The test schematic of the experimental prototype and the thermocouples distribution are illustrated in Fig. 2(b).

Due to the detrimental effect of non-condensable gas, the loop needed to be evacuated to a pressure of 3.0×10^{-4} Pa before being charged. The charge ratio was set to 68.2% of the total system volume for anhydrous ammonia. During the test period, the temperature of the

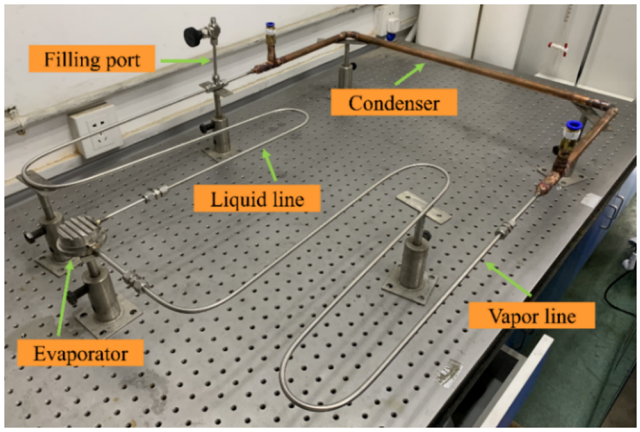

Fig. 3. System diagram of the flat disk LHP.

ambient was maintained around 24 °C, and the allowable vapor temperature at the evaporator outlet was below 40 °C for experimental safety.

3. Results and discussions

3.1. Start-up tests

One of the important operating characteristics is the start-up procedure. A good start-up procedure can indicate the stability and reliability of the LHP. Fig. 4 shows the start-up process at a minimum heat load of 2.5 W with heat sink temperature of −10 °C. The steady rise of the condenser inlet temperature illustrated that the generated vapor in evaporator could smoothly flow into the condenser without impediment. The heater surface temperature also experienced a slight increase. However, due to the low mass flow rate in this operating condition, the effect of the heat leak from the ambient when subcooled working fluid flowed back to the evaporator was inevitably significant. Thus, the evaporator inlet temperature was almost equal to the ambient without suffering any distinct drop.

Fig. 5 shows the start-up process under the maximum allowable heat load of the LHP. The heater surface temperature was 68 °C and the vapor temperature at evaporator outlet reached 40 °C when the loop cycle stabilized. Despite the fact that no further increase in heat load was conducted for experimental safety, the loop almost reached its maximum heat transfer capacity because the heater surface temperature was nearly 70 °C (the maximum operating temperature for most electronic devices). The condenser inlet temperature rose faster compared to the one in Fig. 4 for the mass flow rate increased apparently under high evaporation intensity. In addition, the temperature difference between evaporator outlet and condenser inlet was just 4 °C, but the temperature difference between condenser outlet and evaporator inlet reached up to 11 °C. The cause of such discrepancy was that the vapor flowed faster than the subcooled liquid. Therefore, the heat leak to the ambient in vapor line was much smaller than in liquid line. Furthermore, no temperature pulsation or overshoot was found during the two start-up processes mentioned above.

A particular phenomenon related to the long liquid transport line was found in the start-up tests. Fig. 6(a), (b) and (c) present the start-up processes at three heat loads respectively. The evaporator inlet temperatures went through a similar shift: first a sudden decline occurred, then a fixed value was kept for a time, finally a gradual decrease appeared until reaching stabilization. After each start-up experiment, the evaporator gradually cooled down to the ambient temperature. However, the liquid inside liquid line might remain a cold state due to the heat transfer impediment caused by the thermal insulation material. When heat load was applied to the evaporator again during next test, the remaining working fluid inside vapor channels and vapor chamber evaporated at once, which resulted in a sudden expansion of vapor volume inside vapor line. Such a quick expansion pushed the remaining cold fluid in liquid line towards the evaporator. Thus, the evaporator inlet temperature went through a sharp decrease. While the vapor expansion process was over, the fluid in liquid line started to flow normally and slowly under effect of the capillary force. Nevertheless, the initial driving force of vapor expansion could not push all the liquid into the evaporator. A section of cold liquid, which was in the identical thermal state, was still retained inside the liquid line due to the long length. It might take some time for such a section of liquid to fully flow into the evaporator. Hence, the evaporator inlet would keep at a certain degree of temperature for a while. Only when the new subcooled liquid from the condenser flowed into the evaporator, could the evaporator inlet temperature start to decrease and finally reach a steady state. This process also led to a small overshoot on heater surface temperature. By comparing three operating conditions in Fig. 6, a relation was also found that the time required for the evaporator inlet temperature to stabilize was negatively correlated with the heat load. The larger the heat load, the more intense the vapor expansion and the less of the remaining cold liquid inside the liquid line. Therefore, the shorter time the intermediate temperature maintained and the faster the loop arrived the final state.

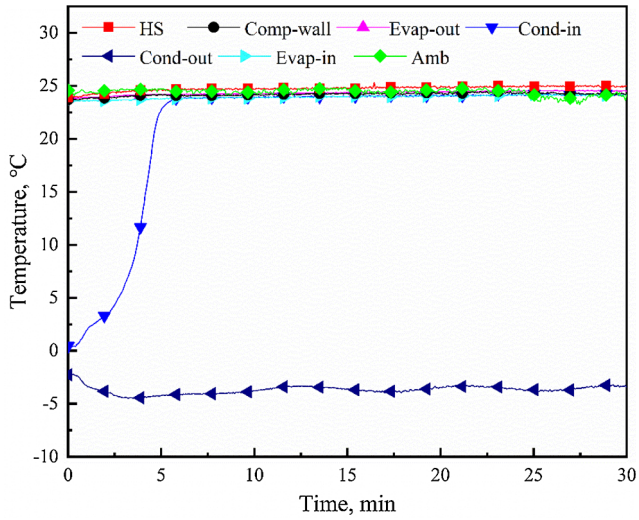

Fig. 4. Start-up process for 2.5 W with heat sink temperature of −10 °C.

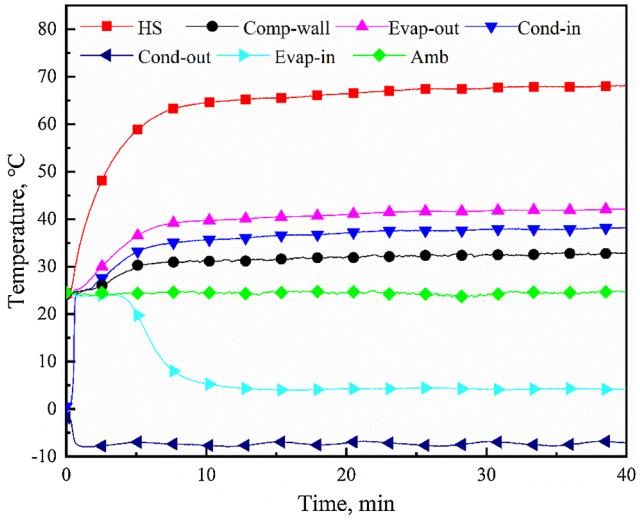

Fig. 5. Start-up process for 180 W with heat sink temperature of −10 °C.

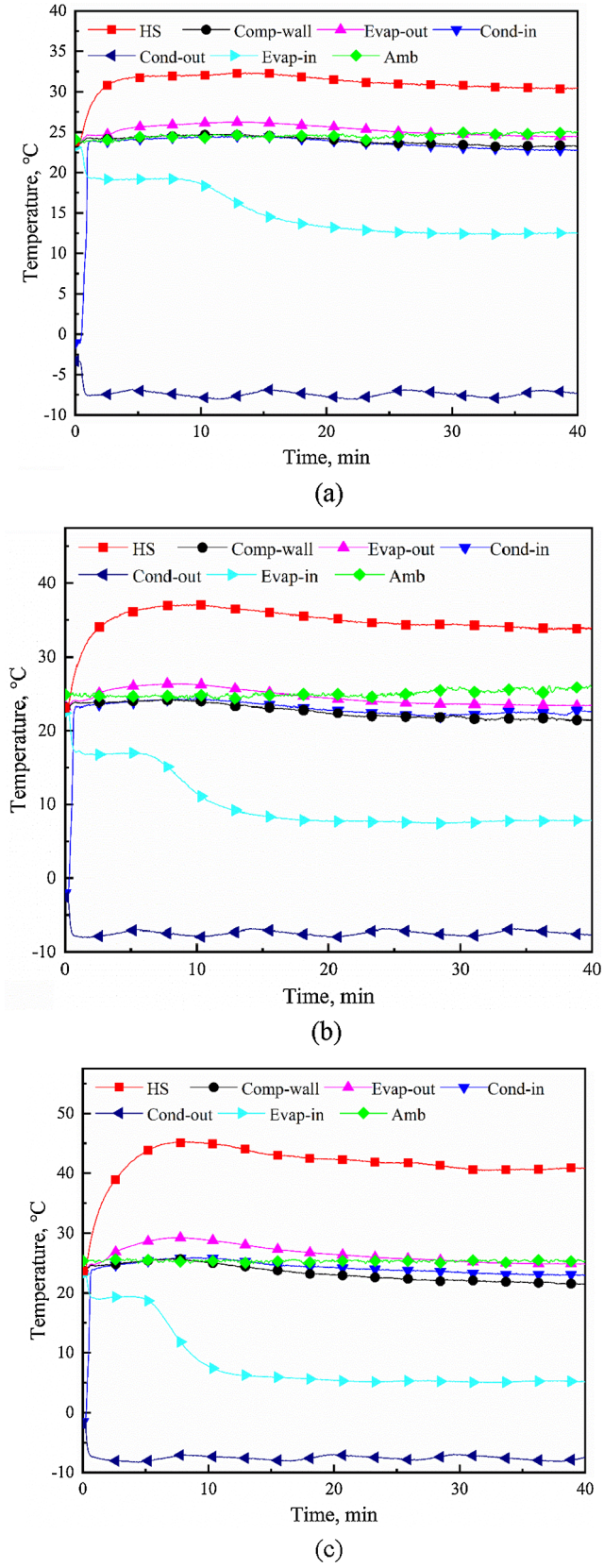

Fig. 6. Start-up process for different heat loads with heat sink temperature of −10 °C. (a) Q = 60 W. (b) Q = 90 W. (c) Q = 120 W.

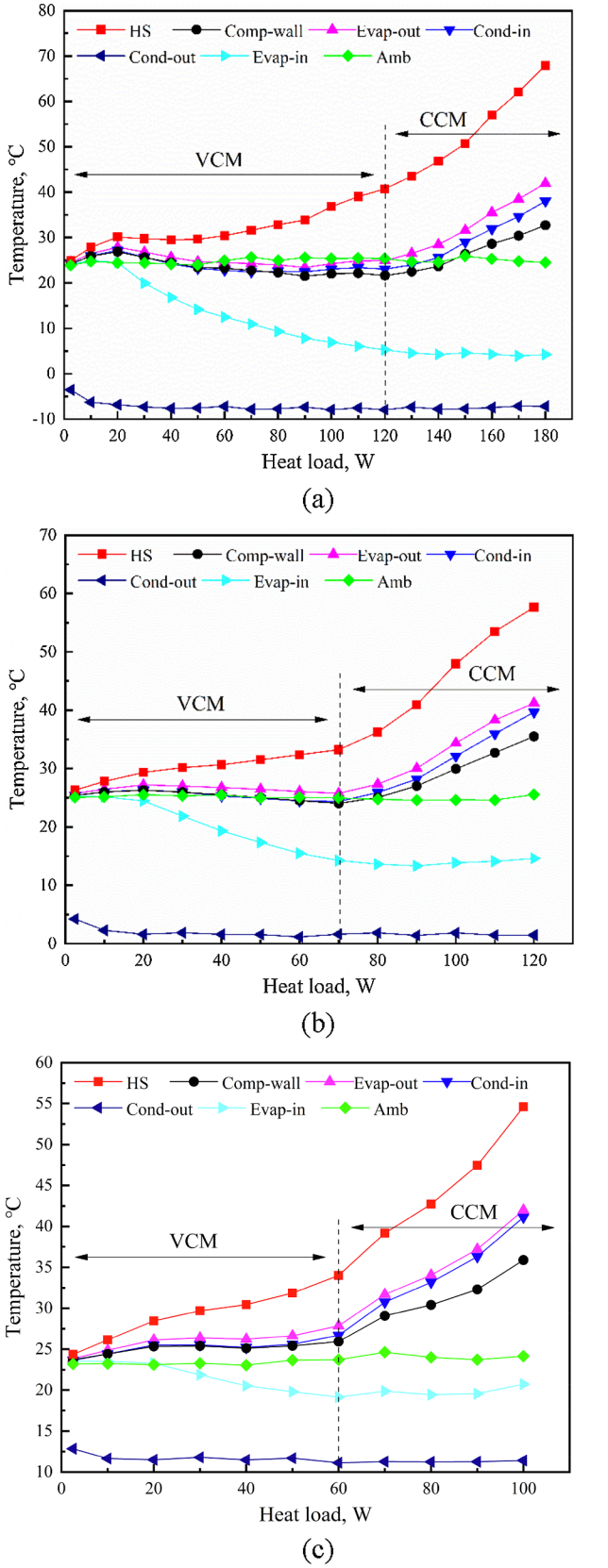

Fig. 7. The temperature distribution of LHP at different heat loads. (a) T_{sink} = -10 °C. (b) T_{sink} = 0 °C. (c) T_{sink} = 10 °C.

3.2. Operating characteristic of LHP

Heat sink temperature is a significant factor that affects LHP operating performance. Fig. 7(a), (b) and (c) present the temperature variation of the loop against heat load at the heat sink temperatures of −10, 0 and 10 °C. The maximum heat load was 180 W when the heat sink temperature was −10 °C, corresponding to the heat flux of 10.8 W/cm^2. The heater surface temperature was 68 °C and the vapor temperature at evaporator outlet reached 40 °C. The minimum heat load that the loop could operate was 2.5 W. As for the anhydrous ammonia, its saturation pressure increased rapidly with temperature. Once the vapor temperature exceeded 40 °C, the pressure inside LHP could be too high to bear. Thus, the vapor temperature should be limited for experimental safety. In addition, the heater surface temperature should be below 70 °C, which was the maximum operating temperature for most electronic devices. Raising the heat sink temperature led to an increase in evaporator inlet temperature, thereby the maximum heat load and the heat transfer capacity of the LHP decreased. For heat sink temperature of 0 °C, the maximum heat load was 120 W (heat flux 7.2 W/cm^2) and the heater surface temperature was 58 °C. For heat sink temperature of 10 °C, the maximum heat load was 100 W (heat flux 6.0 W/cm^2) and the heater surface temperature was 55 °C.

During the experiment, two operation modes, known as variable conductance mode (VCM) and constant conductance mode (CCM), were observed. Two factors, heat leak and flow rate, together determined the operation modes. When the heat sink temperature was −10 °C and the heat load was below 120 W, the loop operated at the variable conductance mode. When heat load added up, the flow rate increased, thus the effect of the heat leak from ambient to subcooled liquid in liquid line reduced and evaporator inlet temperature decreased. However, under the effect of the heat leak from the heater surface, the compensation chamber temperature showed no distinct variation and the heater surface temperature increased slowly. The loop was at variable conductance mode during this period. While further increasing the heat load, the effect of the heat leak in liquid line could not reduce anymore and the evaporator inlet temperature ceased to decrease. The condenser was also fully utilized. Yet the heat leak from the heater surface was too large to be compensated by the subcooled liquid. Therefore, the compensation chamber temperature started to increased and the heater surface temperature rose faster. Hence, the loop switched to the constant conductance mode. Different heat sink temperature also affected the transition heat load for different operation modes. For heat sink temperatures of 0 °C and 10 °C, the transition heat loads were 70 W and 60 W respectively.

3.3. Operation with heat load cycle

For most of the electronic devices, the input power alternation may lead to the variation of heat dissipation requirements, which may affect the reliability of the heat transfer devices. Figs. 8 and 9 show the characteristics of the continuous operation under stepwise and random heat load cycles at heat sink temperature of −10 °C. Before altering the heat loads, the loop should reach the steady state and keep for 10 min. The intermittent operation of the recirculation chiller was the cause of the regular temperature change in condenser outlet. The LHP demonstrated strong reliability at variable heat load and no temperature pulsation or unfavorable overshoot or even operation failure was found. Also, as shown in Fig. 8, when the heat load reduced to below 100 W, the working property was improved than the same operating conditions of the previous period. Compared to the results in Ref. [23], the time required to achieve stability at each heat load was longer because of the longer heat transfer distance.

Two distinct processes, related to the system hysteresis, was described and discussed in detail. One was that when heat load decreased from 120 W to 90 W in Fig. 9, the evaporation intensity suffered a sudden decline. While decreasing the heat load, the long length of liquid line and vapor line inhibited the flow rate from adjusting in time. Large amounts of subcooled liquid flooded into the compensation chamber, causing a significant cooling effect to the evaporator. Thus, the compensation chamber and heater surface temperature dropped excessively, but the evaporator inlet temperature remained the same for a time. As the flow rate decreased, the evaporator inlet temperature started to rise due to the heat leak from the ambient in liquid line and the subcooled degree reduced. Such a small amount of subcooled liquid with low subcooled degree was insufficient to compensate for the heat leak from heater surface to compensation chamber. A new vapor phase started to form inside. The working pressure rose up and the driving force generated on two sides of the capillary menisci in wick would be reduced. Therefore, only by rising the vapor pressure in vapor chamber could the total flow resistance of the loop be balanced. Subsequently, the evaporator outlet temperature and the heater surface temperature began to rise and gradually reached stabilization. Such a phenomenon could also be found in Ref. [18].

The other particular process can be observed in Fig. 9 as well. When heat load decreased from 80 W to 30 W. The compensation chamber and heater surface temperature experienced a dramatic drop and the evaporator inlet temperature was even higher. Unlike the previous process, the compensation chamber and heater surface temperature just gradually stabilized instead of rising again after the sudden decline. In order to indicate the process more specifically, an additional test that the heat load decreased from 140 W to 40 W was carried out. As shown in Fig. 10, the heater surface temperature reduced as the heat load decreased. Besides, due to the much lower heat load, the heat leak from heater surface to compensation chamber could be nearly neglected. Nonetheless, the heat leak from the ambient still existed and the compensation chamber was filled with liquid, which caused the liquid in the compensation chamber to turn into the superheat state with the absence of the vapor phase. The working pressure inside did not rise up and the driving force remained almost the same. On the other hand, the evaporator inlet temperature gradually increased on account of the low flow rate and inevitable environment heat leak. Therefore, the evaporator inlet temperature might exceed the heater surface temperature and maintained stable at such condition. The discrepancy between these two processes was how low the extent that the heat load reduced to. Based on Figs. 8 and 9, if the heat load was greater than 40 W and the vapor phase formed inside compensation chamber, the former process would occur; if the heat load was equal or lower than 40 W and the liquid in compensation chamber turned into superheat state, the latter one would occur instead. This hysteresis phenomenon was also observed and discussed in Ref. [34].

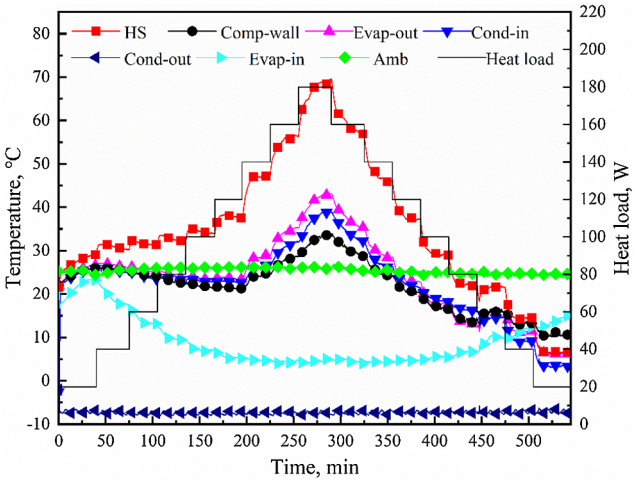

Fig. 8. Continuous operation under stepwise heat load cycle with heat sink temperature of −10 °C.

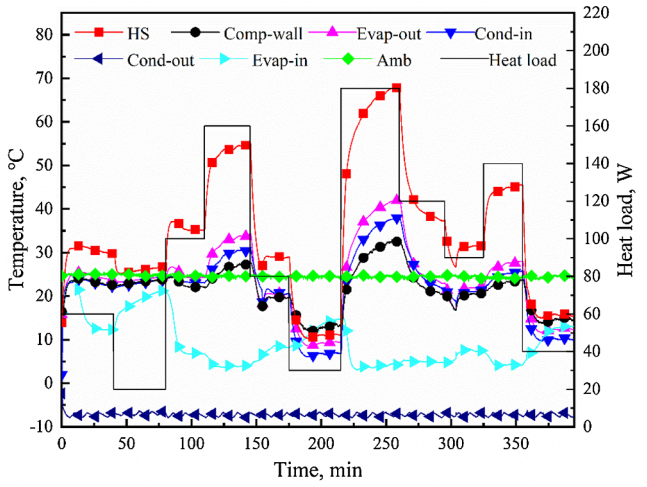

Fig. 9. Continuous operation under random heat load cycle with heat sink temperature of −10 °C.

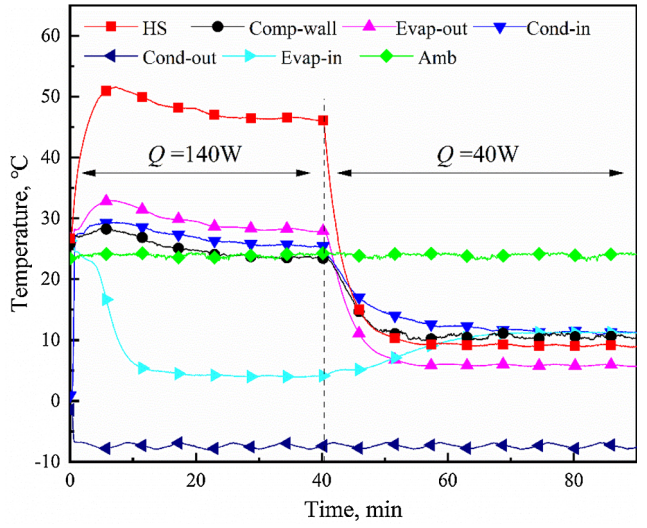

Fig. 10. Variable heat load test with heat sink temperature of −10 °C.

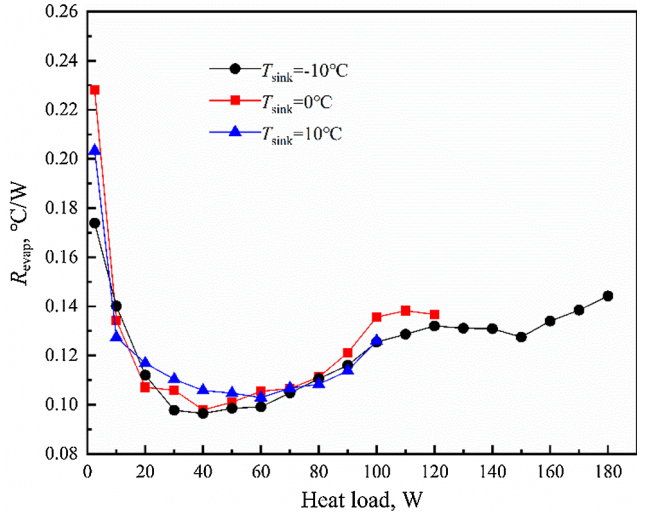

Fig. 11. The evaporator thermal resistances at three heat sink temperature.

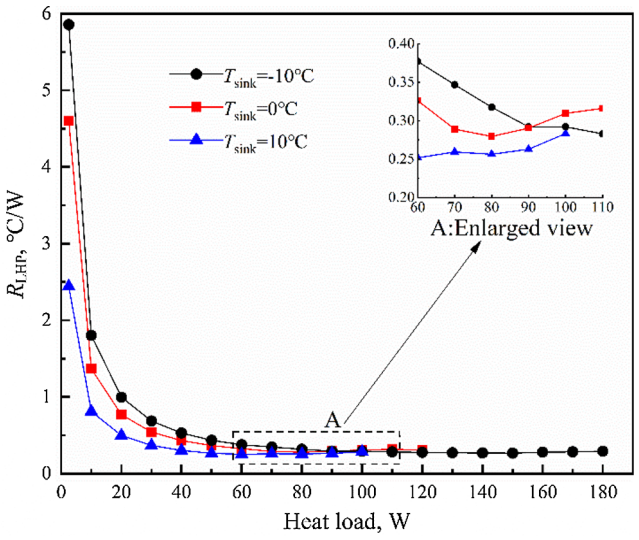

Fig. 12. The LHP thermal resistances at three heat sink temperature.

3.4. Analysis of thermal characteristic

Generally speaking, the evaporator heat transfer capacity can be evaluated by the evaporator thermal resistance, which is defined as

$$R_{evap} = \frac{T_{hs} - T_v}{Q} \tag{2}$$

where T_{hs} is the average temperature measured by two thermocouples at the heater surface. T_v is the vapor temperature at the evaporator outlet and Q is the heat load produced by the input power.

Fig. 11 illustrates the relation for evaporator thermal resistance against heat load at three heat sink temperatures. It was clear to see that with the increase in heat load, the evaporator thermal resistance first dropped rapidly to the minimum value, and then rose until the heat load reaching the maximum value. Also, the lower the heat sink temperature, the smaller the minimum evaporator thermal resistance. For heat sink temperature of −10 °C, the evaporator thermal resistance varied between 0.096 °C/W and 0.174 °C/W, and the minimum value was achieved at the heat load of 40 W. Reason for the variation trend was related to the different vapor–liquid distribution in the wick structure. While the heat load rose up and did not exceed 40 W, the evaporation intensity was increased with an enlargement of vapor-liquid interface. Thus, the heat transfer on the wick surface was intensified and the evaporator thermal resistance reduced. Further rising the heat load, vapor started to generate inside the wick. This resulted in the formation of overheated vapor film and the heat transfer between heater surface and vapor-liquid interface was blocked. Besides, the increase in heat leak from heater surface also caused the formation of vapor phase in compensation chamber, which impeded the liquid supply to the vapor-liquid interface. Therefore, the evaporator heat transfer capacity reduced and the evaporator thermal resistance increased.

As for the whole system thermal characteristic, the evaluation index is the LHP thermal resistance, which can be defined as

$$R_{LHP} = \frac{T_{hs} - T_c}{Q} \tag{3}$$

where T_c is the average temperature of the condenser inlet and outlet. Fig. 12 presents the variation of LHP thermal resistance at different heat loads and heat sink temperatures. As could be seen from the enlarged

view in Fig. 12, The LHP thermal resistance showed a similar trend to that of the evaporator. When rising the heat load, the evaporator heat transfer capacity and condenser cooling efficiency both increased. However, the condenser cooling efficiency reached its maximum and evaporator heat transfer capacity would reduce at high heat load. Thus, before reaching the maximum heat load, the LHP thermal resistance first dropped extremely and then rose slightly. Furthermore, as the heat sink temperature decreased, the LHP thermal resistance increased due to the enlargement of the temperature difference between evaporator and condenser. Overall, in addition to the heat load below 10 W, the LHP thermal resistance varied between 0.252 °C/W and 0.810 °C/W for heat sink temperature of 10 °C and between 0.267 °C/W and 1.802 °C/W for heat sink temperature of −10 °C. And the minimum LHP thermal resistance of 0.252 °C/W was achieved when heat load was 60 W and heat sink temperature was 10 °C.

By means of error analysis, the uncertainty of R_{evap} can be calculated by

$$\frac{\delta R_{evap}}{R_{evap}} = \sqrt{(\frac{\delta y}{y})^2 + (\frac{\delta Q}{Q})^2} \tag{4}$$

$$\delta y = \sqrt{\sum_{i=1}^{2} (\frac{1}{2}\delta T_i)^2 + (\delta T_v)^2} \tag{5}$$

$$y = T_{hs} - T_v \tag{6}$$

where T_i is the temperature at heater surface measured by two thermocouples. Deducing from the accuracy of T-type thermocouples used in the loop, δT_i and δT_v were all equal to 0.5 °C. Thus, the uncertainty of R_{evap} was estimated to be ± 6.12% at low heat load (Q = 10 W) and ± 0.35% at high heat load (Q = 180 W). Similarly, the uncertainty of R_{LHP} was estimated to be ± 5.08% at low heat load (Q = 10 W) and ± 0.31% at high heat load (Q = 180 W).

With the advantages of long heat transfer distance and good thermal characteristics mentioned above, the system herein was considered to have the potential to use in aerospace scenarios. Also, it could satisfy the demand of heat transfer capacity needed for electronic devices in satellites and sustain high operating performance even under variable working conditions and extreme environment.

4. Conclusions

In this paper, a stainless steel-ammonia LHP with a biporous wick and a flat disk evaporator was designed. The heat transfer distance was 1.6 m and the allowable heater surface temperature was below 70 °C. In order to get the operating performance of the loop in detail, a series of studies including start-up and continuous heat load cycle tests were carried out experimentally. The main conclusions could be drawn as below.

1. The LHP could transfer the heat load as much as 180 W (heat flux 10.8 W/cm^2) at heat sink temperature of −10 °C. The heater surface temperature under such operating condition was 68 °C and the vapor temperature at evaporator outlet reached 40 °C. Also, the loop could start up successfully at a minimum heat load of 2.5 W. During the start-up and variable heat load tests, no unfavorable temperature overshoot or pulsation was observed and the LHP demonstrated strong reliability and stability.
2. With the effect of the remaining liquid in liquid line and the initial driving force of vapor expansion during the start-up process, the evaporator inlet temperature first experienced a sudden decline, then maintained a fixed value before a further decline. Meanwhile, the time required for the evaporator inlet temperature to stabilize was negatively correlating with the heat load.
3. Two particular processes, which were related to the status of working fluid in compensation chamber and the synergy of heat leaks from heater surface and long transport line, were found at continuous heat load cycle tests. The distinction between these two processes was whether the compensation chamber and heater surface temperature would rise again after an excessive decline.
4. Two different operation modes, known as variable conductance mode and constant conductance mode, were observed at the whole range of heat load. Except for the heat load below 10 W, the evaporator thermal resistance varied between 0.096 °C/W and 0.144 °C/W at heat sink temperature of −10 °C, and the LHP thermal resistance varied between 0.252 °C/W and 0.810 °C/W at heat sink temperature of 10 °C.

Declaration of Competing Interest

To the best of our knowledge and belief, neither I nor any coauthors have any competing financial interests or personal relationships that could have appeared to influence the work reported in this paper.

Acknowledgements

This work was supported by the National Natural Science Foundation of China (No. 51736004 and No. 51776079).

References

[1] G. Zhou, J. Li, Z. Jia, Power-saving exploration for high-end ultra-slim laptop computers with miniature loop heat pipe cooling module, Appl. Energy 239 (2019) 859–875.
[2] N. Putra, B. Ariantara, R.A. Pamungkas, Experimental investigation on performance of lithium-ion battery thermal management system using flat plate loop heat pipe for electric vehicle application, Appl. Therm. Eng. 99 (2016) 784–789.
[3] H. Zhang, G. Li, L. Chen, G. Man, J. Miao, X. Ren, J. He, Y. Huo, Development of flat-plate loop heat pipes for spacecraft thermal control, Microgravity Sci. Technol. 31 (2019) 435–443.
[4] H. Jouhara, H. Ezzuddin, Thermal performance characteristics of a wraparound loop heat pipe (WLHP) charged with R134A, Energy 61 (2013) 128–138.
[5] S. Becker, S. Vershinin, V. Sartre, E. Laurien, J. Bonjour, Y.F. Maydanik, Steady state operation of a copper-water LHP with a flat-oval evaporator, Appl. Therm. Eng. 31 (2011) 686–695.
[6] Y.F. Maydanik, Loop heat pipes, Appl. Therm. Eng. 25 (2005) 635–657.
[7] W. Joung, T. Yu, J. Lee, Experimental study on the loop heat pipe with a planar bifacial wick structure, Int. J. Heat Mass Transf. 51 (2008) 1573–1581.
[8] L. Bai, J. Fu, G. Lin, C. Zhou, D. Wen, Quiet power-free cooling system enabled by loop heat pipe, Appl. Therm. Eng. 155 (2019) 14–23.
[9] Z. Liu, D. Wang, C. Jiang, J. Yang, W. Liu, Experimental study on loop heat pipe with two-wick flat evaporator, Int. J. Therm. Sci. 94 (2015) 9–17.
[10] Y.F. Maydanik, S. Vershinin, M. Chernysheva, Experimental study of an ammonia loop heat pipe with a flat disk-shaped evaporator using a bimetal wall, Appl. Therm. Eng. 126 (2017) 643–652.
[11] G.P. Celata, M. Cumo, M. Furrer, Experimental tests of a stainless steel loop heat pipe with flat evaporator, Exp. Therm Fluid Sci. 34 (2010) 866–878.
[12] R. Singh, A. Akbarzadeh, M. Mochizuki, Operational characteristics of a miniature loop heat pipe with flat evaporator, Int. J. Therm. Sci. 47 (2008) 1504–1515.
[13] A. Anand, A. Jaiswal, A. Ambirajan, P. Dutta, Experimental studies on a miniature loop heat pipe with flat evaporator with various working fluids, Appl. Therm. Eng. 144 (2018) 495–503.
[14] Y.F. Maydanik, M. Chernysheva, V. Pastukhov, Loop heat pipes with flat evaporators, Appl. Therm. Eng. 67 (2014) 294–307.
[15] K. Odagiri, H. Nagano, Heat transfer characteristics of flat evaporator loop heat pipe under high heat flux condition with different orientations, Appl. Therm. Eng. 153 (2019) 828–836.
[16] V.M. Kiseev, V.V. Vlassov, I. Muraoka, Experimental optimization of capillary structures for loop heat pipes and heat switches, Appl. Therm. Eng. 30 (2010) 1312–1319.
[17] J. Li, D. Wang, G. Peterson, Experimental studies on a high performance compact loop heat pipe with a square flat evaporator, Appl. Therm. Eng. 30 (2010) 741–752.
[18] S. He, Z. Liu, J. Zhao, C. Jiang, J. Yang, W. Liu, Experimental study of an ammonia loop heat pipe with a flat plate evaporator, Int. J. Heat Mass Transf. 102 (2016) 1050–1055.
[19] J.H. Boo, W.B. Chung, Experimental study on the thermal performance of a small-scale loop heat pipe with polypropylene wick, J. Mech. Sci. Technol. 19 (2005) 1052–1061.
[20] T. Semenic, I. Catton, Experimental study of biporous wicks for high heat flux applications, Int. J. Heat Mass Transf. 52 (2009) 5113–5121.
[21] T. Semenic, Y.-Y. Lin, I. Catton, Thermophysical properties of biporous heat pipe evaporators, J. Heat Transf. 130 (2008) 022602.
[22] X. Cao, P. Cheng, T. Zhao, Experimental study of evaporative heat transfer in sintered copper bidispersed wick structures, J. Thermophys. Heat Transf. 16 (2002) 547–552.
[23] B. Chen, W. Liu, Z. Liu, H. Li, J. Yang, Experimental investigation of loop heat pipe

with flat evaporator using biporous wick, Appl. Therm. Eng. 42 (2012) 34–40.
[24] B. Chen, Z. Liu, W. Liu, J. Yang, H. Li, D. Wang, Operational characteristics of two biporous wicks used in loop heat pipe with flat evaporator, Int. J. Heat Mass Transf. 55 (2012) 2204–2207.
[25] K. Nakamura, K. Odagiri, H. Nagano, Study on a loop heat pipe for a long-distance heat transport under anti-gravity condition, Appl. Therm. Eng. 107 (2016) 167–174.
[26] Y. Maydanik, V. Pastukhov, M. Chernysheva, Development and investigation of a loop heat pipe with a high heat-transfer capacity, Appl. Therm. Eng. 130 (2018) 1052–1061.
[27] A.A. Adoni, A. Ambirajan, V. Jasvanth, D. Kumar, P. Dutta, Theoretical and experimental studies on an ammonia-based loop heat pipe with a flat evaporator, IEEE Trans. Compon. Packag. Technol. 33 (2010) 478–487.
[28] N. Atabaki, B.R. Baliga, Experimental investigation of a loop heat pipe with a flat evaporator, in: International Heat Transfer Conference 13, Begel House Inc., 2006.
[29] X. Zhang, J. Huo, S. Wang, Experimental investigation on temperature oscillation in a miniature loop heat pipe with flat evaporator, Exp. Therm. Fluid Sci. 37 (2012) 29–36.
[30] Y. Maydanik, S. Vershinin, M. Chernysheva, The results of comparative analysis and tests of ammonia loop heat pipes with cylindrical and flat evaporators, Appl. Therm. Eng. 144 (2018) 479–487.
[31] D. Wang, Z. Liu, J. Shen, C. Jiang, B. Chen, J. Yang, Z. Tu, W. Liu, Experimental study of the loop heat pipe with a flat disk-shaped evaporator, Exp. Therm Fluid Sci. 57 (2014) 157–164.
[32] M. Kaviany, Principles of Heat Transfer in Porous Media, Springer Science & Business Media, 2012.
[33] H. Li, Z. Liu, B. Chen, W. Liu, C. Li, J. Yang, Development of biporous wicks for flat-plate loop heat pipe, Exp. Therm. Fluid Sci. 37 (2012) 91–97.
[34] S.V. Vershinin, Y.F. Maydanik, Hysteresis phenomena in loop heat pipes, Appl. Therm. Eng. 27 (2007) 962–968.